Technical Report No. 11

CONTINUUM MODELS FOR IRREGULAR PHASE BOUNDARY MOTION IN SHAPE-MEMORY TENSILE BARS

by

Phoebus Rosakis[1] and James K. Knowles[2]

CALIFORNIA INSTITUTE OF TECHNOLOGY

Office of Naval Research

Grant N00014-93-1-0240

Technical Report No. 11

CONTINUUM MODELS FOR IRREGULAR PHASE BOUNDARY MOTION IN SHAPE-MEMORY TENSILE BARS

by

Phoebus Rosakis[1] and James K. Knowles[2]

[1]Department of Theoretical and Applied Mechanics
Cornell University
Ithaca, New York 14853

[2]Division of Engineering and Applied Science
California Institute of Technology
Pasadena, California 91125

November, 1997

CONTINUUM MODELS FOR IRREGULAR PHASE BOUNDARY MOTION IN SHAPE-MEMORY TENSILE BARS

by

Phoebus Rosakis[1] and James K. Knowles[2]

[1]Department of Theoretical and Applied Mechanics
Cornell University
Ithaca, New York 14583

[2]Division of Engineering and Applied Science
California Institute of Technology
Pasadena, California 91125

ABSTRACT

We consider quasi-static displacement-controlled loading through one stress cycle of a shape-memory tensile bar modeled as a one-dimensional, two-phase elastic solid. Our objective is to explore the effect on the associated hysteresis loop of various qualitatively different types of kinetic relations, bearing in mind certain features of such loops that have been observed experimentally. We show that when the model involves a kinetic relation that is "unstable" in a definite sense, "stick-slip" motion of the interface between phases and serration of the accompanying stress-elongation curve are both predicted at slow elongation rates. We also show that a "nonhomogeneous" kinetic relation intended to model the effect of micro-obstacles on interface motion also leads to irregular interface motion and a serrated stress-elongation curve, in this case at *all* elongation rates.

Keywords: hysteresis, kinetic relation, shape-memory, stick-slip.

1. Introduction. When tensile bars composed of shape-memory materials such as NiTi or AgCd are subjected to quasi-static cyclic mechanical loading, hysteresis loops are usually observed; see, for example, Krishnan & Brown (1973), Krishnan (1985), Shaw and Kyriakides (1995). For a given material, the size and other qualitative features of such loops usually change with loading rate and with the temperature at which the test takes place.

According to some simple continuum models of the underlying phase transformation in shape-memory tensile bars, the hysteretic response to slow cyclic loading arises from the dissipation associated with the motion of the sharp interface, or *phase boundary*, between two metastable phases present in the bar; see Abeyaratne & Knowles (1991, 1992). In such models, the velocity of a phase boundary is governed by a kinetic relation, which expresses the jump in the Gibbs free energy per unit reference volume across the interface, denoted here by f, in terms of the phase boundary velocity $\dot{s}$. Usually it is assumed that the kinetic relation is such that f increases with increasing $\dot{s}$ (*monotonic kinetics*) and that the relation between f and $\dot{s}$ is independent of the instantaneous location of the phase boundary (*homogeneous kinetics*). With both of these assumptions in force, the simple models do indeed predict hysteretic behavior, but they do not predict certain experimentally observed features of hysteresis loops, such as the serrations often seen in the load-elongation curves (Krishnan & Brown (1973), Krishnan (1985)), or the accompanying "jerky motion of the transformation front" (Krishnan (1985)). Indeed, in the *thermal* cycling experiments on single crystals of AuCd carried out by Chang (1952), phase boundary velocity as a function of time was found to be "stick-slip" in character.

In the present paper, we show that these latter features may be predicted by the simple models, provided *either* monotonicity *or* homogeneity of the kinetic relation is relinquished.

The effect of abandoning monotonicity while retaining homogeneity of the kinetic relation has been explored by Rosakis & Knowles (1996) in certain problems for shape-memory bars for which inertia is important. In this reference, it is shown that significant qualitative changes in the dynamic response predicted by the simple models result from non-monotonic kinetics. In particular, phase boundary motion caused by impact at the end of an elastic bar may be of stick-slip type under these conditions, in contrast to the smooth phase boundary advance predicted by a monotonic, homogeneous kinetic relation. A physical argument suggesting that a

non-monotonic kinetic relation may be appropriate for rapidly propagating phase boundaries in certain martensitic transformations was given by Owen, Schoen & Srinivasan (1970).

In fracture mechanics, the counterpart of a kinetic relation is the relation between fracture toughness and crack-tip velocity. Non-monotonic versions of the latter relation, which lead to stick-slip crack-tip motion, have been inferred from experiments as well as predicted by various models. A particular model of this kind and a review of relevant literature have been given by Webb & Aifantis (1995).

In what follows, we examine the predicted response of bars to displacement-controlled quasi-static loading in the same purely mechanical context employed by Rosakis & Knowles (1996), inertial and thermal effects being suppressed. In the next section, we describe the one-dimensional model on which our discussion is based. In Section 3, we determine the predictions of the model for displacement-controlled loading and unloading when the kinetic relation is both monotonic and homogeneous. With such conventional kinetics, the model is capable of exhibiting rate-dependence of the stress-response as well as either load-drop or load-rise upon nucleation, but the predicted phase boundary motion is smooth, and there is no serration in the stress-elongation curves. Section 4 is concerned with the effect of *non-monotonic* but homogeneous kinetics for the same loading program. Here it is found that, for sufficiently small elongation rates, phase boundary motion is of stick-slip type, and the stress-elongation curves are serrated, while at intermediate or high loading rates, phase boundary motion is smooth and there are no serrations. Finally, in Section 4 we study *non-homogeneous* but monotonic kinetics that crudely model the effect on phase boundary motion of defects at the microscale. In this model, jerky motion of the phase boundary and serration of the stress-elongation curve occur at all elongation rates, although stick-slip interface motion arises only for small loading rates.

2. The model. Consider a nonlinearly elastic bar that occupies the interval [0, L] of the x-axis in the reference configuration. In an equilibrium deformation, the particle at x in the reference state is carried to x + u(x), where u is the displacement, and $\gamma(x) = u'(x)$ is the corresponding strain. The nominal stress $\sigma(x)$ acting on the particle located at x in the reference state is related to $\gamma(x)$ by the relation

$$\sigma = \hat{\sigma}(\gamma) \equiv W'(\gamma), \quad \gamma > -1, \tag{2.1}$$

where $W(\gamma)$ is the strain energy per unit volume at the strain γ; the restriction $\gamma > -1$ assures that the deformation is one-to-one. For elastic materials capable of existing in more than one phase, the relation (2.1) between stress and strain is not monotonic; see Ericksen (1975). For a two-phase elastic material, the simplest such relation corresponds to the "trilinear" stress-strain curve shown in Figure 1. The two rising portions of this curve correspond to the stress response of the two metastable phases of the material; they are described by

$$\sigma = \hat{\sigma}(\gamma) = \begin{cases} \mu\,\gamma, & -1 < \gamma < \gamma_M, \\ \mu\,(\gamma - \gamma_T), & \gamma > \gamma_m. \end{cases} \tag{2.2}$$

Here μ is Young's modulus, which is taken to be the same in both phases for simplicity, and $\gamma_T > 0$ is the transformation strain from the low-strain phase ($-1 < \gamma < \gamma_M$) to the high-strain phase ($\gamma > \gamma_m$). In this simple model, γ_T is independent of stress. The declining branch of the stress-strain curve represents the unstable phase of the material.

For equilibrium in the absence of body forces, the stress σ must be independent of x. If σ is between σ_m and σ_M (Figure 1), the corresponding strain need not be constant, even though $\sigma'(x) \equiv 0$. In particular, one may have an equilibrium mixture with two metastable phases separated by a phase boundary whose referential position is, say, x = s; for definiteness, suppose

that the high-strain phase is to the left of the phase boundary, while the particles for which $s \le x < L$ are in the low-strain phase. For a stress σ in this range, the respective strains γ^-, γ^+ in the high- and low-strain phases are found from (2.2) to be

$$\gamma^- = \gamma_T + \sigma/\mu, \quad \gamma^+ = \sigma/\mu \, . \tag{2.3}$$

The Gibbs free energy per unit reference volume is $G(\gamma, \sigma) = W(\gamma) - \sigma\,\gamma$. Bearing in mind that σ is constant along the bar, the jump in G across the phase boundary at $x = s$ is equal to

$$f = W(\gamma^+) - W(\gamma^-) - \sigma\,(\gamma^+ - \gamma^-) = \int_{\gamma^-}^{\gamma^+} \hat{\sigma}(\gamma)\, d\gamma - \sigma\,(\gamma^+ - \gamma^-); \tag{2.4}$$

f is the *driving force* per unit cross-sectional area of the bar acting on the phase boundary (Abeyaratne & Knowles (1991)). Computing the area under the stress-strain curve involved in $(2.4)_2$ and making use of (2.3) leads to

$$f = \gamma_T(\sigma - \sigma_*), \tag{2.5}$$

where $\sigma_* = (\sigma_M + \sigma_m)/2$ is the *Maxwell stress* for the material; σ_* is the stress that cuts off triangles A and B of equal area from the stress-strain curve of Figure 1.

In this mixed-phase state, the overall elongation of the bar is given by

$$\delta = \gamma^-\, s + \gamma^+(L - s) = \sigma L/\mu + \gamma_T\, s \, ; \tag{2.6}$$

when $s = 0$, the bar is entirely in the low-strain phase, while it is in the high-strain phase when $s = L$.

Now consider a *quasi-static process*, in which stress, strain, phase boundary location and elongation in the formulas above are functions of time: $\sigma = \sigma(t)$, $\gamma^{\pm} = \gamma^{\pm}(t)$, $s = s(t)$, $\delta = \delta(t)$. In such a process, the difference

$$D(t) = \sigma(t)\,\dot{\delta}(t) - d/dt \int_0^L W(\gamma(x, t))\,dx. \tag{2.7}$$

is the *dissipation rate*. One can show that $D(t) = f(t)\,\dot{s}(t)$, where $f(t)$ is the driving force per unit area at time t as in (2.4) and $\dot{s}(t)$ is the phase boundary velocity; see Abeyaratne & Knowles (1991). The second law of thermodynamics then requires that

$$f(t)\,\dot{s}(t) \geq 0. \tag{2.8}$$

Now suppose, for example, that the elongation history $\delta(t)$ is prescribed. From (2.6), it is clear that $\sigma(t)$ cannot be determined from a knowledge of elongation history alone; $s(t)$ must be known as well. To remove this indeterminacy, one imposes a *kinetic relation* connecting f and $\dot{s}$: $f(t) = \varphi(\dot{s}(t), s(t))$, where the kinetic response function φ is a characteristic of the material. If φ does not depend on $s(t)$, the kinetics are said to be *homogeneous*:

$$f(t) = \varphi(\dot{s}(t)); \tag{2.9}$$

we shall in fact assume that the kinetic relation is homogeneous as in (2.9) until Section 5. The dissipation inequality (2.8) imposes the requirement

$$\varphi(\dot{s})\,\dot{s} \geq 0 \tag{2.10}$$

on the function φ. For simplicity, we shall assume throughout that $\varphi(\dot{s})$ is odd in $\dot{s}$.

In any loading program that begins with the bar in the reference configuration, the entire specimen will remain in the low-strain phase until a phase transition nucleates. We take $x = 0$ to be the nucleation site, so that upon nucleation, a phase boundary will emerge at $x = 0$ and move into the bar in accordance with the kinetic relation (2.9), the high-strain phase being on the left, as assumed in (2.6). The nucleation criterion is taken to be a critical level f_c of driving force per unit area acting on the incipient phase boundary; in view of (2.5), there is a corresponding critical nucleation stress $\sigma_c = \sigma_* + f_c/\gamma_T$ and hence a critical elongation $\delta_c = \sigma_c L/\mu$ as well. Note that the "entropy inequality" (2.8) requires that $f_c \geq 0$ when the nucleation site is at $x = 0$; thus necessarily $\sigma_c \geq \sigma_*$. If loading continues after the phase change nucleates until the phase boundary reaches $x = L$, the bar is fully transformed, and in further loading, the bar behaves as a linearly elastic material with the properties of the high-strain material phase. If the loading is then reversed, the bar will eventually nucleate the reverse transition from the high-strain to the low-strain phase. We take the nucleation site for the reverse transition to be $x = L$, and for simplicity we choose the nucleation level of driving force per unit area to be $- f_c$; the corresponding nucleation stress and critical elongation are $\sigma_* - f_c/\gamma_T$ and $L\gamma_T + (L/\mu)(\sigma_* - f_c/\gamma_T)$, respectively.

3. Hysteresis for monotonic and homogeneous kinetics. We now implement the model described above for a program of loading in which the specimen is at first extended at a given constant elongation rate $\dot{\delta}$ from the reference state until the bar is fully transformed, after which the elongation rate is changed to $-\dot{\delta}$, and the bar is shortened until the stress returns to zero.

When the kinetic response function $\varphi(\dot{s})$ increases monotonically with $\dot{s}$, one may write the kinetic relation (2.9) in the inverted form

$$\dot{s} = \Phi(f), \tag{3.1}$$

where $\Phi = \varphi^{-1}$. By eliminating f and s among (2.5), (2.6) and (3.1), one obtains a first order, ordinary differential equation for the stress $\sigma(t)$ that applies from the instant of nucleation $t = 0$ until the phase boundary has completely traversed the specimen:

$$\dot{\sigma} = \frac{\mu}{L}\dot{\delta} - \frac{\mu\gamma_T}{L}\,\Phi(\gamma_T(\sigma - \sigma_*)). \tag{3.2}$$

The initial condition to accompany (3.2) is

$$\sigma = \sigma_c \quad \text{when } t = 0. \tag{3.3}$$

After the reverse transformation is nucleated during unloading, one replaces $\dot{\delta}$ by $-\dot{\delta}$ in (3.2) to obtain the appropriate differential equation, and (3.3) is replaced by the condition corresponding to nucleation of the reverse transformation.

To illustrate the hysteretic behavior associated with monotonic and homogeneous kinetics, we consider the special case of the kinetic relation (2.9) for which

$$\varphi(\dot{s}) = \begin{cases} f_r + (1/\omega)\dot{s} & \text{for } \dot{s} > 0, \\ -f_r + (1/\omega)\dot{s} & \text{for } \dot{s} < 0, \end{cases} \tag{3.4}$$

where the material constants f_r and ω are the resistance to phase boundary motion and the phase boundary *mobility*, respectively. Here $0 \le f_r \le f_c$, and $0 < \omega \le \infty$; dimensionally, ω is a velocity per unit stress. The graph of φ is shown schematically in Figure 2. For this kinetic relation, the initial value problem (3.2), (3.3) becomes

$$\dot{\sigma} + \frac{\mu\gamma_T^2\omega}{L}(\sigma - \sigma_r) = \frac{\mu}{L}\ddot{\delta}, \qquad \sigma = \sigma_c \text{ at } t = 0, \tag{3.5}$$

where we have set $\sigma_r = \sigma_* + f_r/\gamma_T$. The load-elongation curve that follows upon solving this initial value problem, together with the corresponding one for unloading, is shown schematically in Figure 3 for two elongation rates. As one readily sees from (3.5), if $\sigma_c > \sigma_r$ as assumed in the figure, then for small enough elongation rates, the stress decreases after nucleation during loading; otherwise, stress increases monotonically throughout the loading portion of the program.

4. Unstable kinetic relations. To study the effect of non-monotonic kinetics, we now suppose that the kinetic response function $\varphi(\dot{s})$ in (2.9) is odd in $\dot{s}$ and has the following properties:

$$\left.\begin{aligned} &\varphi(0+) = \varphi(b) = f_c, \quad \varphi'(0+) < 0, \quad \varphi'(a) = 0, \\ &\varphi''(\dot{s}) \geq 0 \quad \text{for } \dot{s} > 0, \quad \varphi'(\dot{s}) \begin{cases} < 0 & \text{for } 0 < \dot{s} < a, \\ > 0 & \text{for } \dot{s} > a\,. \end{cases} \end{aligned}\right\} \tag{4.1}$$

Such a non-monotonic $\varphi(\dot{s})$ is shown schematically in Figure 4. We view $\varphi(\dot{s})$ as set-valued at $\dot{s} = 0$: $\varphi(0) = [-f_c, f_c]$. When φ has these properties, we call the kinetic response function *unstable*. For convenience, we assume that the nucleation level of driving force per unit area f_c and the resistance to phase boundary motion f_r coincide: $f_c = f_r$.

Kinetic relations that are unstable in the above sense were investigated by Rosakis & Knowles (1996) for dynamic impact problems in tensile bars.

It is convenient to retain the differential equation for $\sigma(t)$ in the form (3.2), even though the inverse kinetic response function Φ is multiple-valued when φ is as shown in Figure 4. For an unstable kinetic response function, the curve in the σ, $\dot{\sigma}$-plane described by (3.2) is shown in Figure 5 for three cases:

$$\left.\begin{array}{ll} \text{Case a:} & \dot{\delta} > \gamma_T\, b/L \quad \text{(high elongation rate)}, \\ \text{Case b:} & \gamma_T\, a/L < \dot{\delta} < \gamma_T\, b/L \quad \text{(intermediate elongation rate)}, \\ \text{Case c:} & 0 < \dot{\delta} < \gamma_T\, a/L \quad \text{(low elongation rate)}. \end{array}\right\} \tag{4.2}$$

The constants a and b appearing in (4.2) are defined in (4.1); see Figure 4. The arrows in Figure 5 indicate the sense in which the trajectory would be traversed with increasing time if all points on the trajectory were accessible. Thus above the σ-axis, $\dot{\sigma} > 0$, so σ increases, while below, the motion is to the left. The fact that Φ is multiple-valued gives rise to a lack of uniqueness; for some ranges of σ, there are three possible values of $\dot{\sigma}$. In order to pick a unique solution of (3.2), we adopt the convention, sometimes called *perfect delay* (Poston & Stewart (1978)), which asserts that $\dot{\sigma}(t)$ will jump at an instant $t = t_*$ only when there is no alternative, in the sense that (3.2) has no solution with $\dot{\sigma}(t)$ continuous in an open interval containing t_*. Thus during the loading portion of the constant-elongation-rate process under consideration, the system evolves as shown in Figure 6 for each of the three cases in (4.2). In Figures 6(a) and 6(b), the point with coordinates $\sigma = \sigma_\infty$, $\dot{\sigma} = 0$ corresponds to an equilibrium state of (3.2) and would represent the long-time limit of the solution of the associated initial value problem for loading if the differential equation were applicable for all time. In cases (a) and (b), the stress in the bar at first increases at the constant rate $\mu\dot{\delta}/L$ as the curve in Figure 6(a) or (b) is traversed from point A to point B. Nucleation of the high-strain phase then occurs, and $\dot{\sigma}$ decreases discontinuously, corresponding to a jump from B to C. At the high elongation rates (case (a)), the stress then increases along CD, moving toward the equilibrium point, but stopping when the bar is fully transformed, at which time unloading would commence. At the intermediate elongation rates (Figure 6(b)), the stress *decreases* along CD until the transformation is complete. At the low elongation rates (Figure 6(c)), nucleation at the point B is followed by a jump in $\dot{\sigma}$, after which the stress decreases until the point D is reached, at which time $\dot{\sigma}$ jumps again, reaching the value

$\mu\dot{\delta}/L$ at the point E. The stress now increases at this constant rate along EB; during this portion of the loading process, (3.2), (3.1) show that $\dot{s} = 0$, so that the phase boundary is at rest until the stress reaches the value σ_c at the point B. The stress rate $\dot{\sigma}$ then jumps again, the phase boundary resumes its advance, and the cycle BCDEB is traversed again. This process gives rise to oscillations in $\sigma(t)$: during the passage from E to B, the phase boundary is stationary as $\sigma(t)$ increases, while CD corresponds to decreasing stress and an advancing phase boundary. The motion of the phase boundary is thus of "stick-slip" type at the low elongation rates of case (c), corresponding to the "jerky motion of the transformation front" observed in the experiments described by Krishnan (1985) and leading to the serrations in the load-elongation curve mentioned earlier. In the experimental results for a CuSn alloy reported in Figure 18 of Nakanishi (1975), serrations in the load- elongation curve appear to occur at low elongation rates but not at higher ones. On the other hand, data for NiTi wires shown in Figure 2 of Lin, Tobushi et al. (1996) indicate the presence of serrations over three decades of elongation rate at three different temperatures.

The stress-elongation curves associated with the processes just described are shown schematically in Figure 7 for the three different regimes of elongation rate (4.2). In the serrated part of the curve for the low elongation rate, the "stick" portions are parallel to the stress-strain curves of the pure phases ($\sigma = \mu\gamma$ and $\sigma = \mu(\gamma - \gamma_T)$). One can show that, in the limit $\dot{\delta} \to 0$ of vanishing elongation rate, the "slip" portions of the curve are asymptotically vertical. Also, the number of serrations during the loading process decreases with increasing elongation rate.

The unloading process, with nucleation and growth of the low-strain phase, can be analyzed in a similar way.

5. Non-homogeneous kinetic relations. We now consider the case in which the kinetic response function depends on the instantaneous location of the phase boundary, so that the

kinetic relation is

$$f = \varphi(\dot{s}, s). \tag{5.1}$$

We shall assume that $\varphi(\dot{s}, s)$ increases monotonically with $\dot{s}$ for each s, so that (5.1) may be inverted to write $\dot{s} = \Phi(f, s)$, where $\Phi(\cdot, s)$ is now single-valued. We shall be concerned with the example for which

$$f = \varphi(\dot{s}, s) = \begin{cases} f_r(s) + (1/\omega)\,\dot{s}, & \dot{s} > 0, \\ -f_r(s) + (1/\omega)\,\dot{s}, & \dot{s} < 0, \end{cases} \qquad \dot{s} = \Phi(f, s) = \begin{cases} \omega\left[f - f_r(s)\right], & f > f_r(s), \\ 0, & -f_r(s) \le f \le f_r(s), \\ \omega\left[f + f_r(s)\right], & f < -f_r(s). \end{cases} \tag{5.2}$$

where the mobility ω is constant, and $f_r(s) > 0$ is the resistance to motion encountered by the phase boundary when it is located at x = s. The value of driving force per unit area required for nucleation of the low-strain - to - high-strain transition at x = 0 is taken to be $f_c = f_r(0)$.

Again we shall consider a loading program in which the bar is first extended at a constant elongation rate $\dot{\delta}$ until it is fully transformed, after which it is shortened at the elongation rate $-\dot{\delta}$ until the stress returns to zero. As in the preceding section, we shall limit attention to the loading part of the program; an entirely similar analysis applies to unloading. Using (2.5), $(2.6)_2$ to rewrite the portion of (5.2) appropriate to loading in terms of $\dot{s}$, s and δ rather than $\dot{s}$, s and f yields

$$\dot{s} = \begin{cases} \dfrac{\mu\gamma_T}{L}\,\omega\left(\dot{\delta} - \delta_r(s)\right), & \delta > \delta_r(s), \\ 0, & \delta < \delta_r(s), \end{cases} \tag{5.3}$$

where we have set

$$\delta_r(s) = \frac{L}{\mu\gamma_T} f_r(s) + \gamma_T s + \frac{\sigma_*}{\mu} L. \tag{5.4}$$

To illustrate, we choose a special "sawtooth" distribution of resistance to phase boundary motion defined as follows:

$$f_r(s) = f_c - m(s - j\, s_0) \quad \text{for } j\, s_0 \le s < (j+1)s_0, \quad j = 0, 1, 2,..., \tag{5.5}$$

where $f_c > 0$, the slope $m > 0$ and the spatial "period" $s_0 > 0$ are given material constants, with $f_m \equiv f_c - m s_0 \ge 0$; see Figure 8. We view this $f_r(s)$ as mimicking, at the macroscopic level, an intermittent sudden increase in resistance to phase boundary motion due to impediments at the microscale, such as defects or inhomogeneities. When $f_r(s)$ is given by (5.5), the relation (5.4) becomes

$$\delta_r(s) = \delta_r^{(j)}(s) \equiv L\gamma_c + (\gamma_T - n)\, s + j\, n\, s_0 \ , \quad j\, s_0 \le s < (j+1)\, s_0, \quad j = 0, 1, 2, \ldots \ , \tag{5.6}$$

where

$$\gamma_c = \frac{f_c + \gamma_T \sigma_*}{\mu\gamma_T}, \quad n = \frac{mL}{\mu\gamma_T}. \tag{5.7}$$

In physical terms, γ_c is the strain, measured in units of the transformation strain γ_T, suffered by the particle $x = 0$ upon nucleation of the high-strain phase, and n is a dimensionless version of the slope of the sawtooth distribution of resistance to phase boundary motion.

Since $\dot{s} = \dot{\delta}\, ds/d\delta$, (5.3) and (5.6) provide a differential equation for $s = s(\delta)$ applicable after nucleation:

$$\rho \frac{ds}{d\delta} = \left\{ \begin{array}{l} \dfrac{\delta}{L} - (\gamma_T - n)\dfrac{s}{L} - \gamma_c - j\, n \dfrac{s_0}{L}, \quad \delta > \delta_r^{(j)}(s) \\ \\ 0, \quad \delta \le \delta_r^{(j)}(s), \end{array} \right\}, \quad j s_0 \le s < (j+1)s_0, \quad j = 1, 2, \ldots, \qquad (5.8)$$

where the dimensionless elongation rate ρ is defined by

$$\rho = \frac{\dot{\delta}}{\mu \gamma_T \omega}. \qquad (5.9)$$

By (5.6), the requirement $s(\delta_r(0)) = 0$ furnishes the initial condition for (5.8):

$$s = 0 \quad \text{for} \quad \frac{\delta}{L} = \gamma_c. \qquad (5.10)$$

For brevity, we shall only consider the case $\gamma_T - n > 0$. It is convenient to introduce dimensionless versions of s, s_0 and δ by writing

$$\bar{s} = \frac{(\gamma_T - n)^2}{\rho}\frac{s}{L}, \quad \bar{s}_0 = \frac{(\gamma_T - n)^2}{\rho}\frac{s_0}{L}, \quad \bar{\delta} = \frac{\gamma_T - n}{\rho}\left(\frac{\delta}{L} - \gamma_c\right), \qquad (5.11)$$

The initial value problem (5.8), (5.10) then becomes

$$\frac{d\bar{s}}{d\bar{\delta}} = \left\{ \begin{array}{l} \bar{\delta} - \bar{\delta}_r(\bar{s}) \quad \text{for} \quad \bar{\delta} > \bar{\delta}_r(\bar{s}), \\ \\ 0 \quad \text{for} \quad \bar{\delta} < \bar{\delta}_r(\bar{s}), \end{array} \right. \qquad \bar{s} = 0 \quad \text{for} \quad \bar{\delta} = 0, \qquad (5.12)$$

where in (5.12) we have set

$$\bar{\delta}_r(\bar{s}) \equiv \bar{\delta}_r^{(j)}(\bar{s}) = \bar{s} + j\frac{n}{\gamma_T - n}\bar{s}_0\,, \quad j\bar{s}_0 \le \bar{s} < (j+1)\bar{s}_0, \quad j = 0, 1, \ldots \quad . \tag{5.13}$$

Consider first the restriction of this initial value problem to the interval $0 \le \bar{s} < \bar{s}_0$, so that $j = 0$ in (5.13):

$$\frac{d\bar{s}}{d\bar{\delta}} = \left\{ \begin{array}{ll} \bar{\delta} - \bar{s} & \text{for} \quad \bar{\delta} > \bar{s}, \\ 0 & \text{for } \bar{\delta} < \bar{s}, \end{array} \right\} \quad 0 \le \bar{s} < \bar{s}_0\,, \quad \bar{s} = 0 \quad \text{for} \quad \bar{\delta} = 0. \tag{5.14}$$

The solution to this problem is

$$\bar{s} = F(\bar{\delta}) \equiv \bar{\delta} + e^{-\bar{\delta}} - 1 \quad \text{for } 0 \le \bar{s} < \bar{s}_0\,. \tag{5.15}$$

(Since necessarily $\bar{\delta} \ge 0$, it is clear in (5.15) that $\bar{\delta} > \bar{s}$ for $0 \le \bar{s} < \bar{s}_0$, and hence that the first of the two alternatives on the right in (5.14) always applies.) The function $F(\bar{\delta})$ in (5.15) is monotonically increasing and convex. There is a unique positive $\bar{\delta} = \Delta(\bar{s}_0)$ such that $F(\bar{\delta}) = \bar{s}_0$. One can show that $\Delta(\bar{s}_0)$ increases monotonically from zero to infinity as $\bar{s}_0$ increases over this range, but $\Delta(\bar{s}_0)/\bar{s}_0$ is monotonically decreasing with $\bar{s}_0$, tending to infinity as $\bar{s}_0 \to 0$ and to unity as $\bar{s}_0 \to \infty$. These properties of $\Delta(\bar{s}_0)$ imply that there are two cases: in case (a), one has $\bar{s}_0 < \Delta(\bar{s}_0) < \bar{s}_0\gamma_T/(\gamma_T - n)$, while for case (b) $\Delta(\bar{s}_0) \ge \bar{s}_0\gamma_T/(\gamma_T - n)$. Figure 9 displays schematic curves described by $\bar{s} = F(\bar{\delta})$ and $\bar{\delta} = \bar{\delta}_r(\bar{s})$ in each of the two cases. The curves OA and OD represent $\bar{s} = F(\bar{\delta})$ in cases (a) and (b), respectively. In case (a), continuation of the solution to the initial value problem (5.12) beyond $\bar{s} = \bar{s}_0$ into the interval $\bar{s}_0 \le \bar{s} < 2\bar{s}_0$ (i.e., for $j = 1$) requires

that $\bar{s}(\bar{\delta})$ be constant in the interval $\Delta(\bar{s}_0) \le \bar{\delta} \le \bar{s}_0\gamma_T/(\gamma_T - n)$, after which the curve OA is "translated" to BC, shown dashed in Figure 9(a). In case (b), the continuation is accomplished by solving the differential equation (5.8) for $j = 1$ subject to an initial condition that corresponds to the point D in Figure 9.

Cases (a) and (b) correspond to different ranges of the dimensionless parameter $\bar{s}_0$; for a given material, $(5.11)_2$ shows that these ranges in turn correspond to different ranges of the dimensionless elongation rate ρ. Indeed, one can show that case (a) arises for low elongation rates $\rho < \rho_c$, case (b) for high rates $\rho > \rho_c$; the critical dimensionless elongation rate ρ_c is given by $\rho_c = \gamma_T(\gamma_T - n)(s_0/L)\Delta_c^{-1}$, where $\Delta = \Delta_c$ is the unique positive root of the equation

$$\frac{\gamma_T}{n}(1 - e^{-\Delta}) = \Delta. \tag{5.16}$$

In case (a), continuation of the solution beyond $\bar{s} = 2\bar{s}_0$ is carried out by further translations of the curve corresponding to (5.15), leading to more intervals of constant $\bar{s}(\bar{\delta})$. In case (b), continuation is accomplished by solving further initial value problems for (5.8), with $j \ge 2$.

The trajectories $s = s(\delta)$ constructed by the process described above are shown schematically in the plane of the physical variables δ and s in Figure 10. It is of interest to note that the motion of the phase boundary is of stick-slip type at low elongation rates (case (a)); indeed, one can show that - as suggested by (5.8), (5.6) - the trajectory $s = s(\delta)$ coincides with the locus $\delta = \delta_r(s)$ in the limit $\dot{\delta} \to 0$. At the higher rates of case (b), the motion, though "jerky", is not stick-slip.

Finally, the relation between stress and elongation during the extensional part of the loading cycle may now be obtained by using the solution $s = s(\delta)$ just constructed in (2.6): $\sigma = \mu(\delta/L - s(\delta)/L)$. After nucleation of the high-strain phase during loading, the σ-δ relation

may be written in terms of the dimensionless variables introduced in (5.11) as

$$\sigma = \sigma_c + \frac{\mu\rho}{\gamma_T - n}\left(\bar{\delta} - \frac{\gamma_T}{\gamma_T - n}\bar{s}(\bar{\delta})\right). \tag{5.17}$$

During the initial period of post-nucleation loading for which $\bar{s} < \bar{s}_0$ and $\bar{\delta} < \Delta(\bar{s}_0)$, (5.15) applies, so that (5.17) may be written in the form

$$\sigma = \sigma_c + \frac{\mu\rho}{\gamma_T - n}\, G(\bar{\delta}), \quad 0 \le \bar{\delta} < \Delta(\bar{s}_0), \tag{5.18}$$

where

$$G(\bar{\delta}) = \frac{\gamma_T}{\gamma_T - n}(1 - e^{-\bar{\delta}}) - \frac{n}{\gamma_T - n}\bar{\delta}. \tag{5.19}$$

One shows readily that $G(0) = 0$, $G'(0) = 1$, G is concave and that G has a maximum at $\bar{\delta} = \bar{\delta}_M \equiv \log(\gamma_T/n)$. One can show $\bar{\delta}_M$ lies in the interval $0 < \bar{\delta} < \Delta(\bar{s}_0)$ if and only if the dimensionless elongation rate ρ satisfies $\rho < \rho_M$, where

$$\rho_M = \frac{(\gamma_T - n)^2}{\log(\gamma_T/n) + n/\gamma_T - 1}\,\frac{s_0}{L}. \tag{5.20}$$

Using the fact that $\gamma_T > n$, one can further show that $\rho_M > \rho_c$, where ρ_c is the dimensionless elongation rate below which stick-slip motion occurs; recall the discussion leading to (5.16). Thus so far as the stress-elongation relation is concerned, there are three regimes of elongation rate:

$$\left.\begin{array}{l} \text{Case i:} \quad 0 < \rho < \rho_c \quad \text{(low elongation rate)} \\ \text{Case ii:} \quad \rho_c < \rho < \rho_M \quad \text{(intermediate elongation rate),} \\ \text{Case iii:} \quad \rho > \rho_M \quad \text{(high elongation rate).} \end{array}\right\} \tag{5.21}$$

The properties of G, together with the continuations of $\bar{s} = \bar{s}(\bar{\delta})$ described above, allow us to draw the stress-elongation curves for loading as shown schematically in Figure 11. Figure 11(a) corresponds to the low elongation rates of case i; the straight portions of the curve on which s = constant such as AB, CD, etc. correspond to the "stick" parts of the phase boundary motion shown in Figure 9(a) or Figure 10(a). These intervals of linearly elastic behavior do not occur in the stress response at the intermediate or high elongation rates of Figure 11(b, c). For intermediate loading rates (case ii), the stress-elongation curve still has multiple local maxima and minima (Figure 11b); the phase boundary moves jerkily but without sticking. At high loading rates (Figure 11c), the stress-elongation curve becomes a monotonic, though still exhibiting multiple discontinuities in slope. Note that serrations are present in the stress-elongation curve at all elongation rates, in contrast to the situation for unstable kinetics found in Section 4, where serrations disappear at sufficiently high loading rates.

Acknowledgments

The authors have had the benefit of many helpful conversations with Rohan Abeyaratne. Financial support during the course of this work from the U.S. National Science Foundation (PR) as well as the U.S. Office of Naval Research (JKK) is also gratefully acknowledged .

References

Abeyaratne, R., Knowles, J.K., 1991, On the driving traction acting on a surface of strain discontinuity in a continuum, *Journal of the Mechanics and Physics of Solids*, **38**, 345-360.

Abeyaratne, R., Knowles, J.K., 1992, Nucleation, kinetics and admissibility criteria for propagating phase boundaries, In *Shock-Induced Transitions and Phase Structures in General Media,* Volume 52 of *IMA Volumes on Mathematics and its Applications*, Eds. R. Fosdick, E. Dunn and M. Slemrod, pp. 1-33, Springer-Verlag, Berlin.

Chang, L.-C., 1952, On diffusionless transformation in Au-Cd single crystals containing 47.5 atomic per cent Cadmium: Characteristics of single-interface transmission, *Journal of Applied Physics*, **23**, 725-728.

Ericksen, J.L., 1975, Equilibrium of bars, *Journal of Elasticity*, **5**, 191-201.

Krishnan, R.V., 1985, Stress induced martensitic transformations, *Materials Science Forum*, **3**, 387-398.

Krishnan, R.V., Brown, L.C., 1973, Pseudo-elasticity and the strain-memory effect in an Ag-45 at. pct. Cd alloy, *Metallurgical Transactions,* **4**, 423-429.

Lin, H.K., Tobushi, H., Tanaka, K., Hattori, T., Ikai, A., 1996, Influence of strain rate on deformation properties of TiNi shape memory alloy, *JSME International Journal*, Series A, **39**, 117-123.

Nakanishi, N., 1975, Lattice softening and the origin of SME, in *Shape Memory Effects in Alloys*, Ed. J. Perkins, pp. 147-176, Plenum Press, New York and London.

Owen, W.S., Schoen, F.J., Srinivasan, G.R., 1970, The growth of a plate of martensite, in *Phase Transformations*, Ed. H.I. Aaronson, pp. 157-180, American Society of Metals, Menlo Park, OH.

Poston, T., Stewart, I.N., 1978, *Catastrophe Theory and its Applications*, Pitman, London.

Rosakis, P., Knowles, J.K., 1996, Unstable kinetic relations and the dynamics of solid-solid phase transitions, Technical Report No. 10, Office of Naval Research Grant N00014-93-1-0240, California Institute of Technology; to appear in *Journal of the Mechanics and Physics of Solids.*

Shaw, J.A., Kyriakides, S., 1995, Thermomechanical aspects of NiTi, *Journal of the Mechanics and Physics of Solids*, **43** , 1243-1281.

Webb, T.W., Aifantis, E.C., 1995, Oscillatory fracture in polymeric materials, 1995, *International Journal of Solids and Structures*, **32,** 2725-2743.

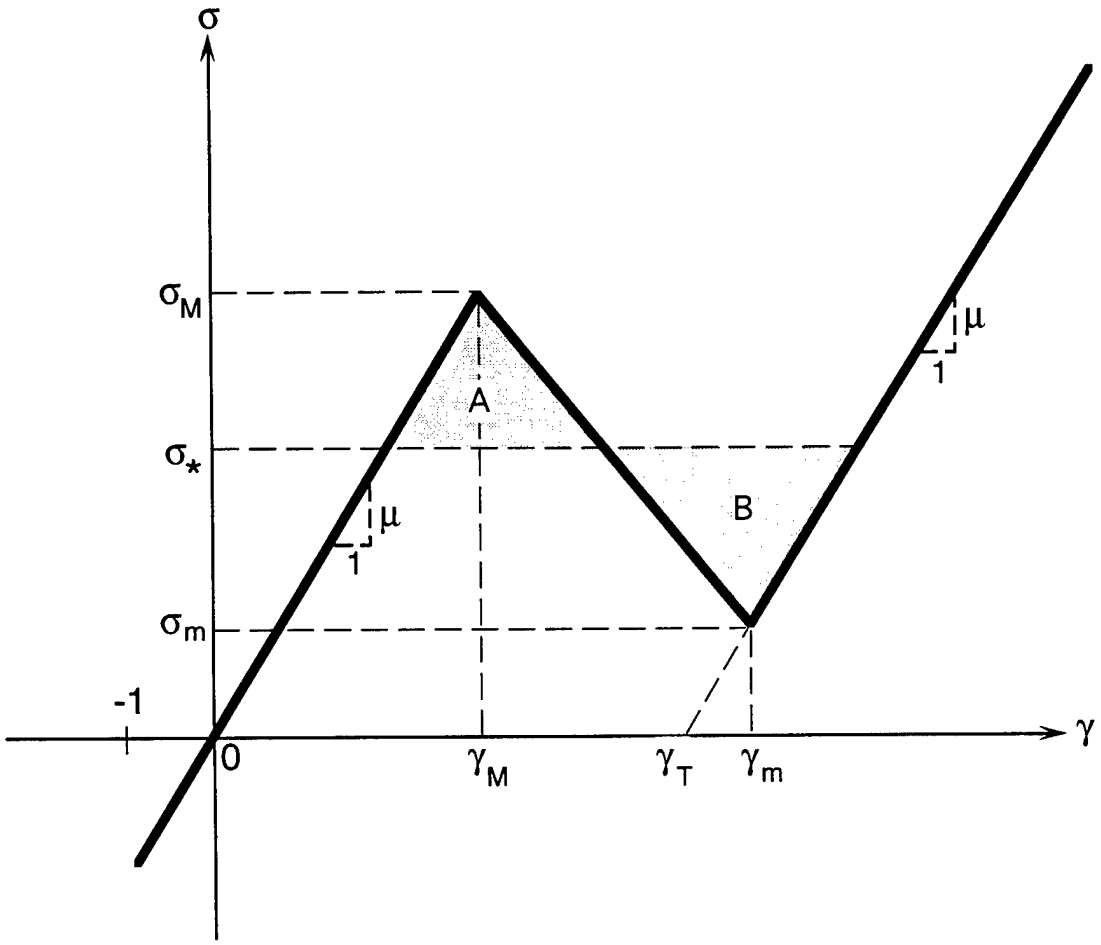

Figure 1. The trilinear elastic material.

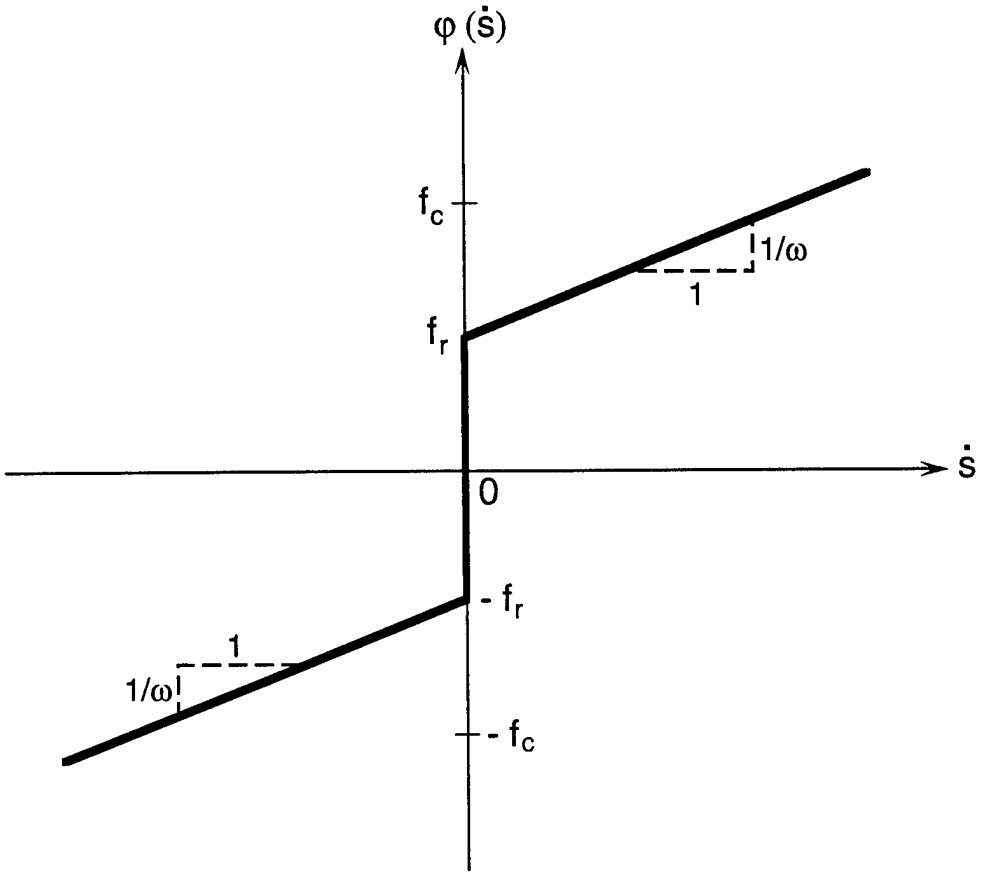

Figure 2. Monotonic, homogeneous kinetic relation.

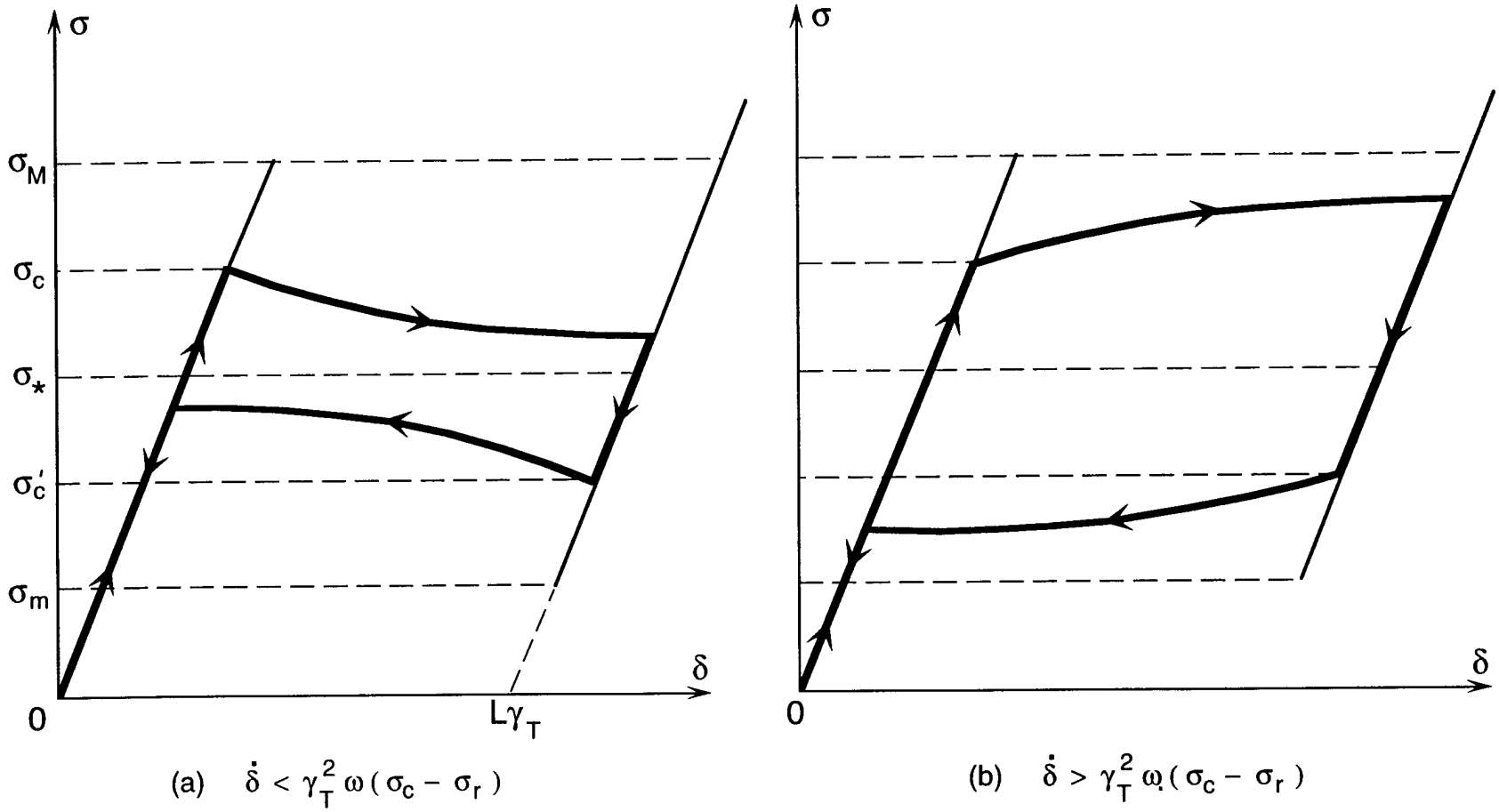

Figure 3. Hysteresis with monotonic, homogeneous kinetics. (a) slow cycling (b) fast cycling.

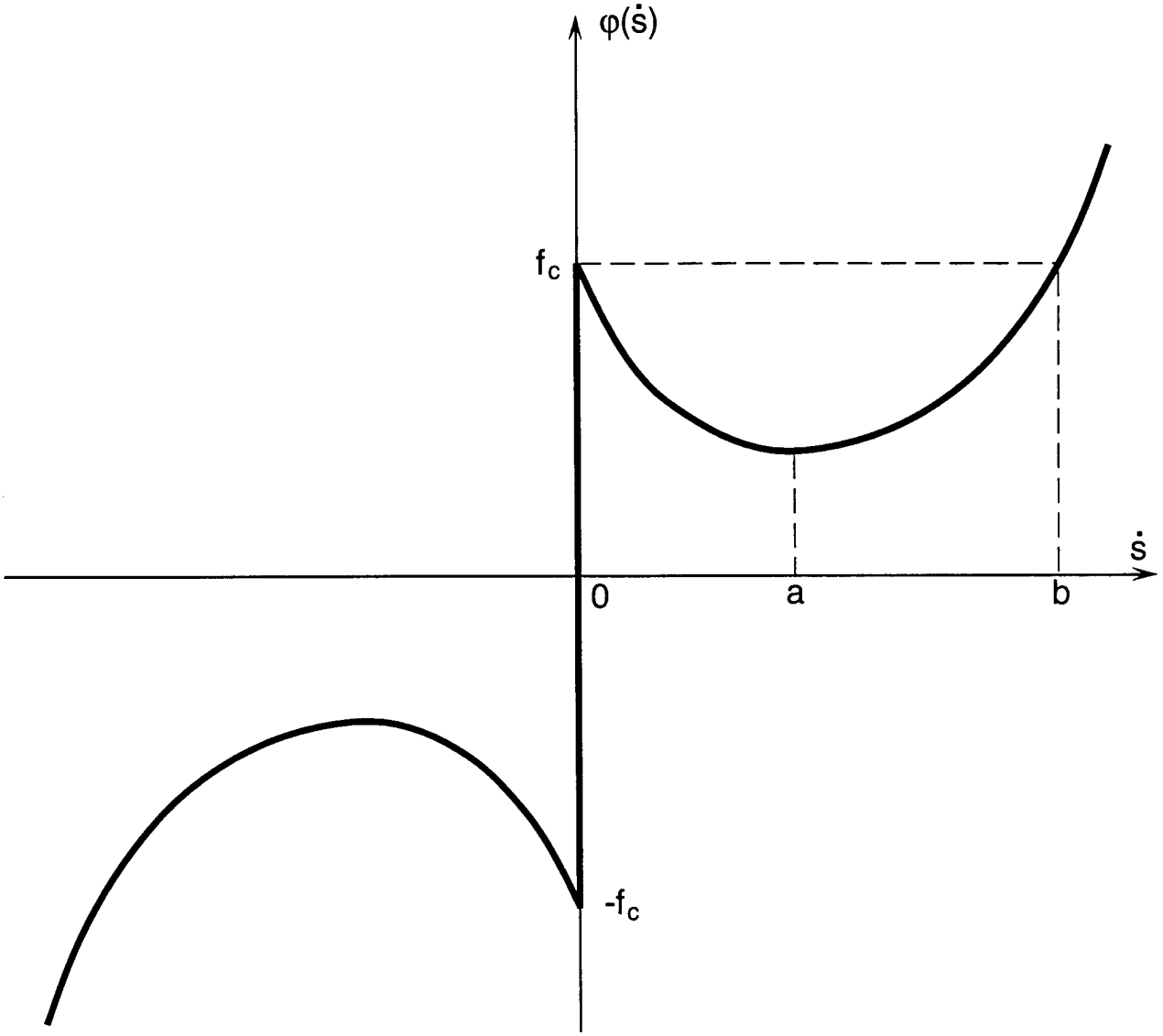

Figure 4. Unstable kinetic response function $\varphi(\dot{s})$.

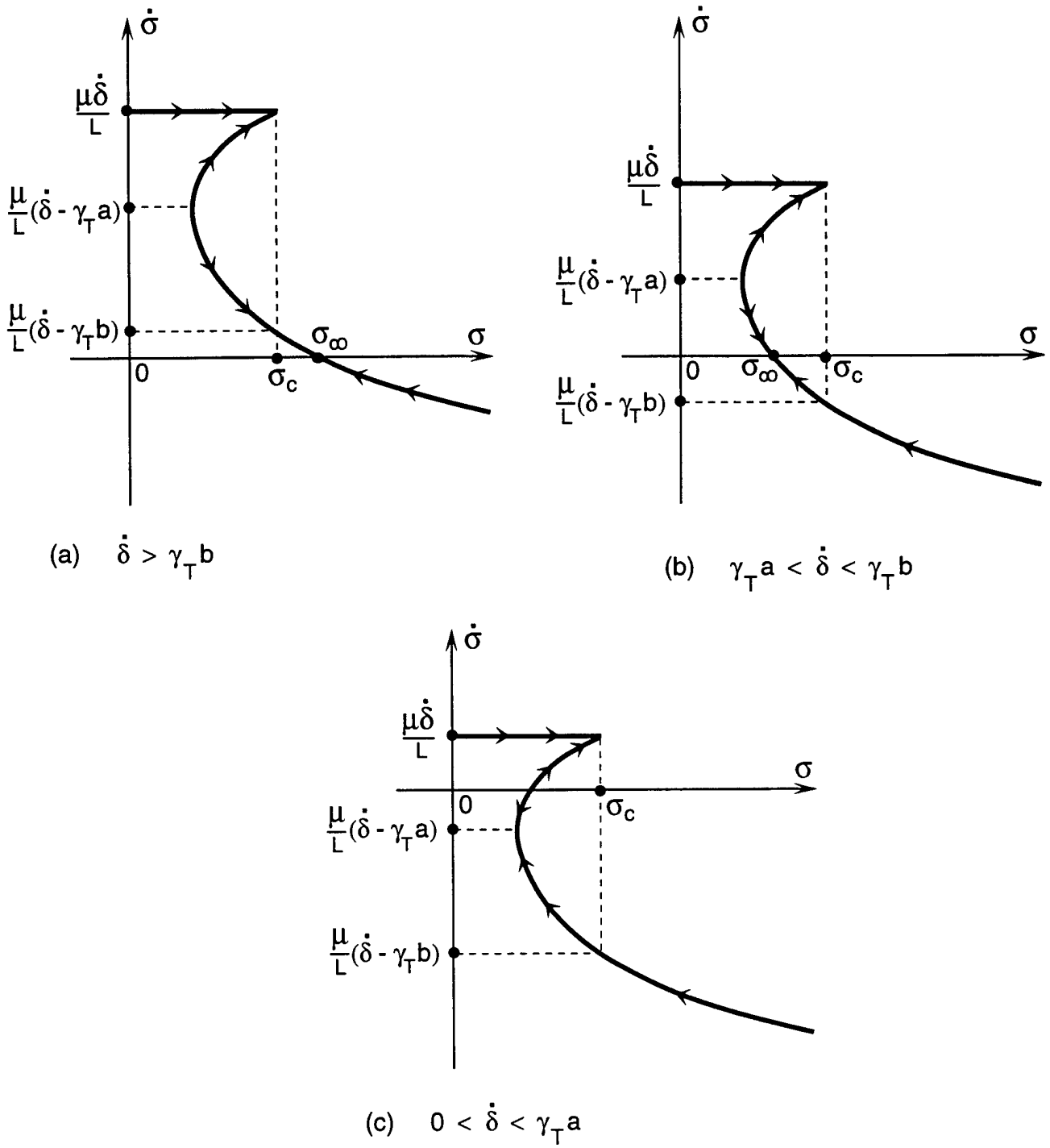

Figure 5. Graphical representation of equation (3.2) for unstable kinetics. Elongation rate is (a) high (b) intermediate (c) low.

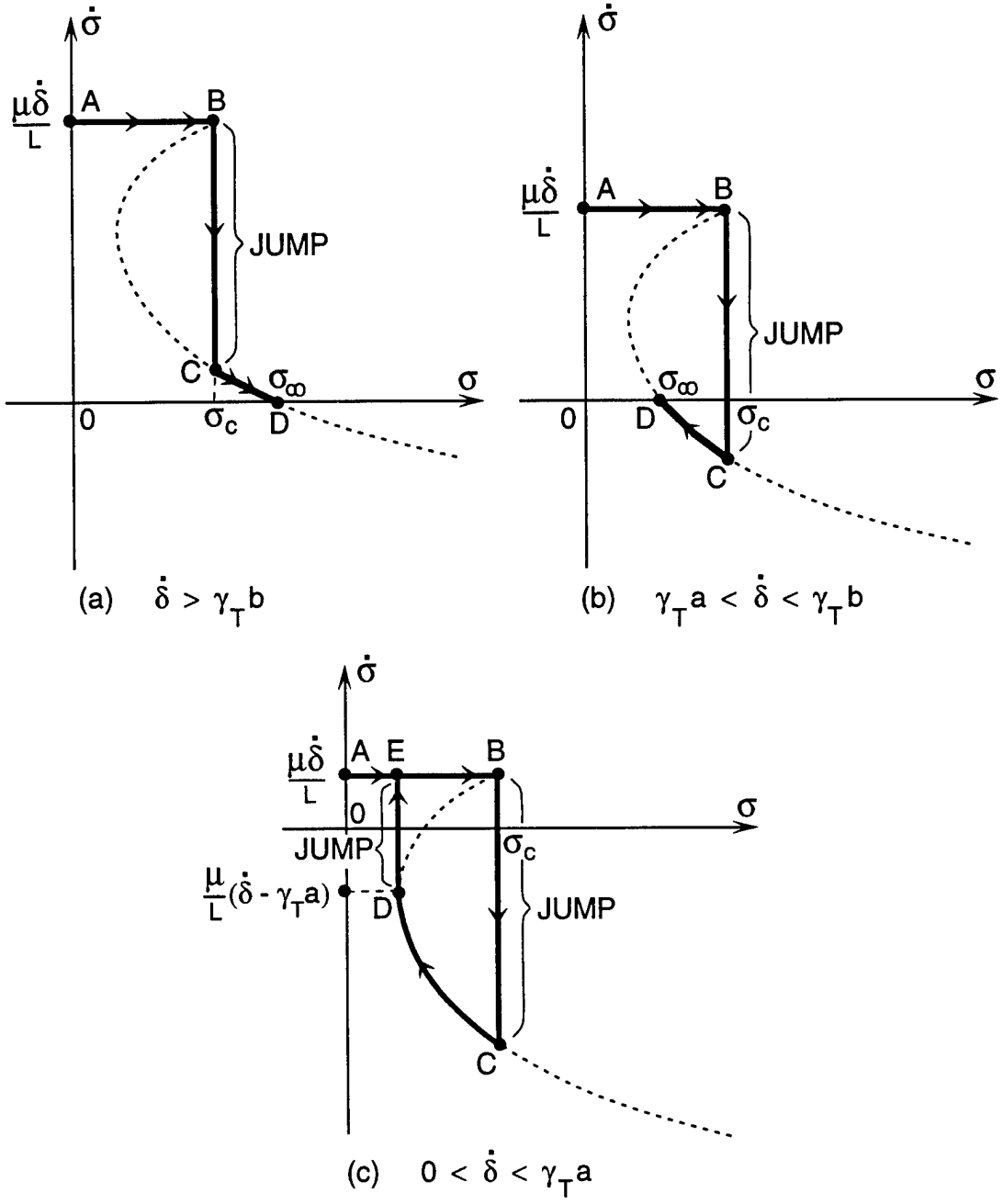

Figure 6. Trajectories of equation (3.2) for unstable kinetics with perfect delay. Elongation rate is (a) high (b) intermediate (c) low.

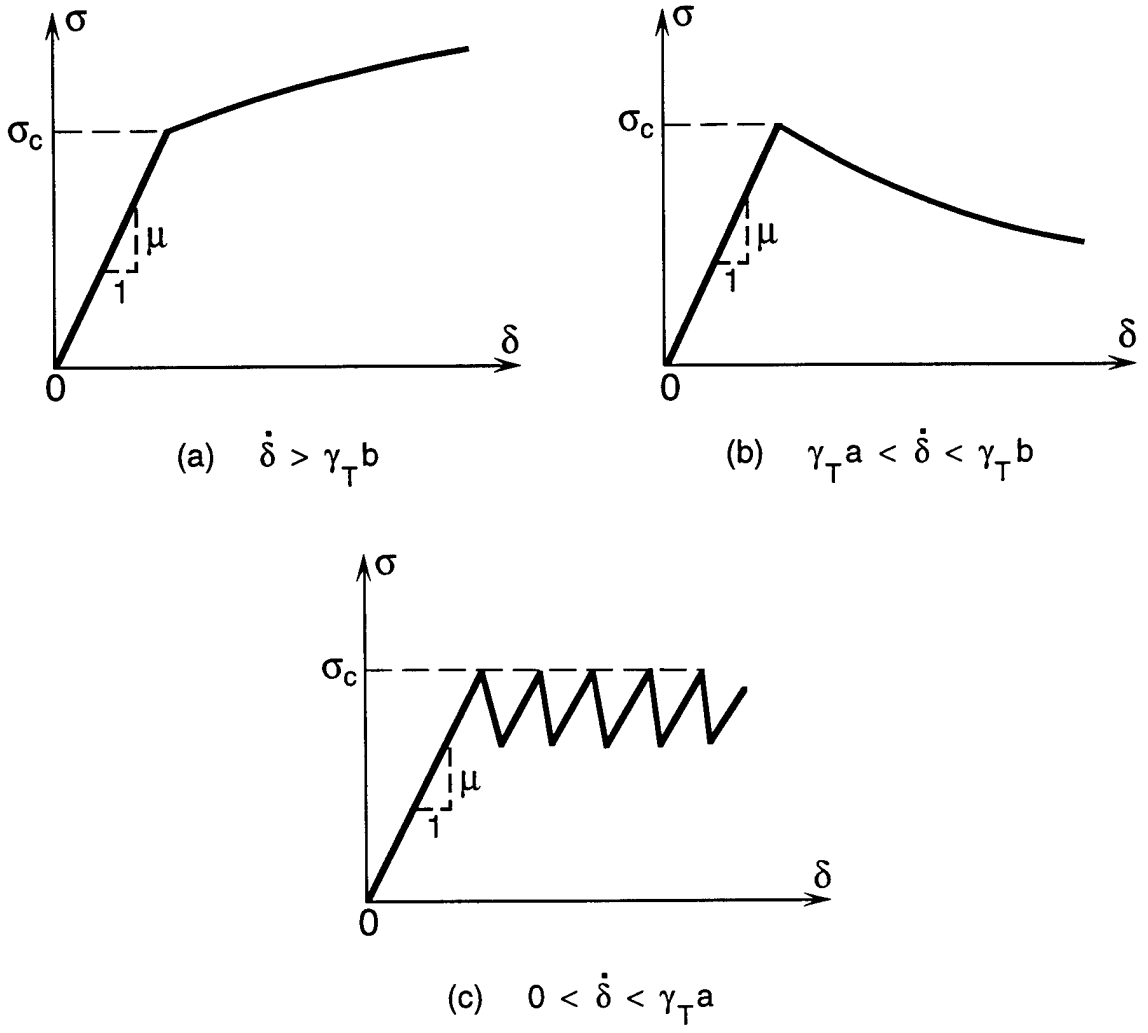

Figure 7. Stress - elongation curves for unstable kinetics with perfect delay. Elongation rate is (a) high (b) intermediate (c) low.

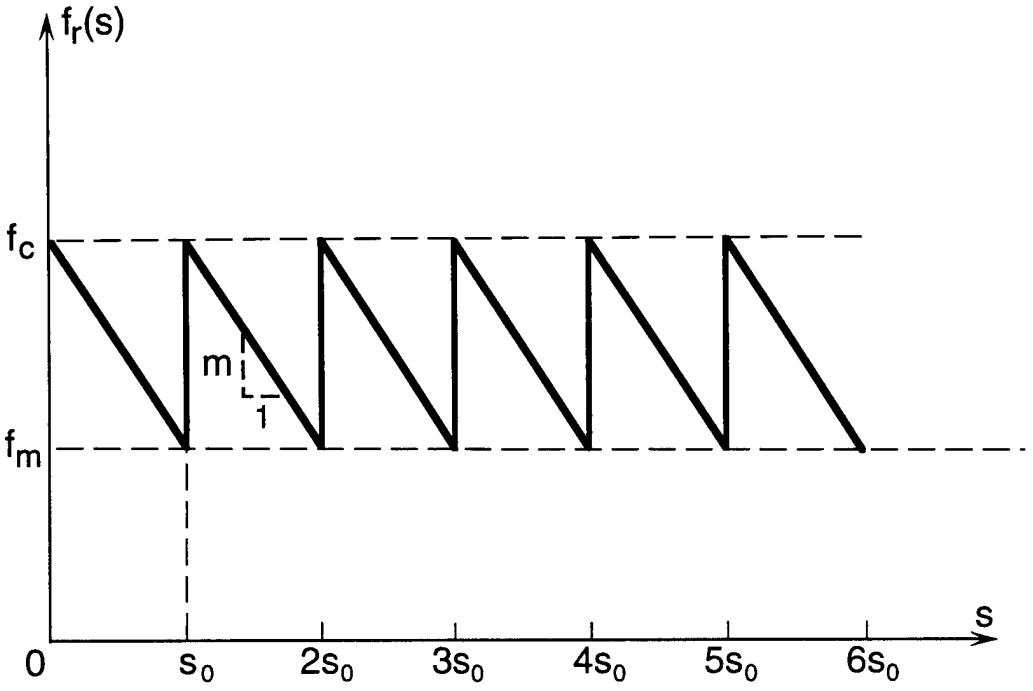

Figure 8. Sawtooth distribution of resistance to phase boundary motion.

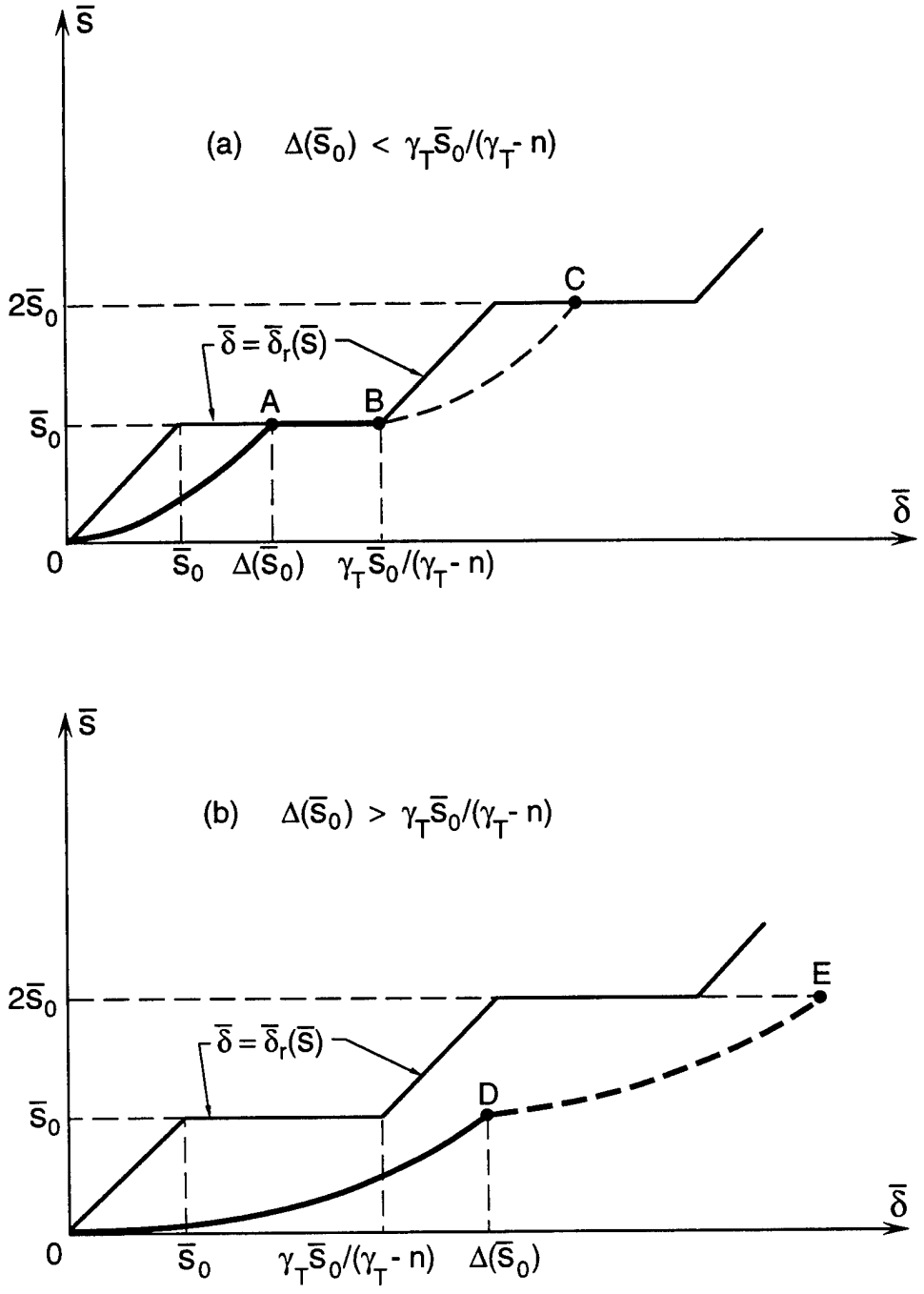

Figure 9. Trajectories corresponding to (5.16), (a) low elongation rate (b) high elongation rate.

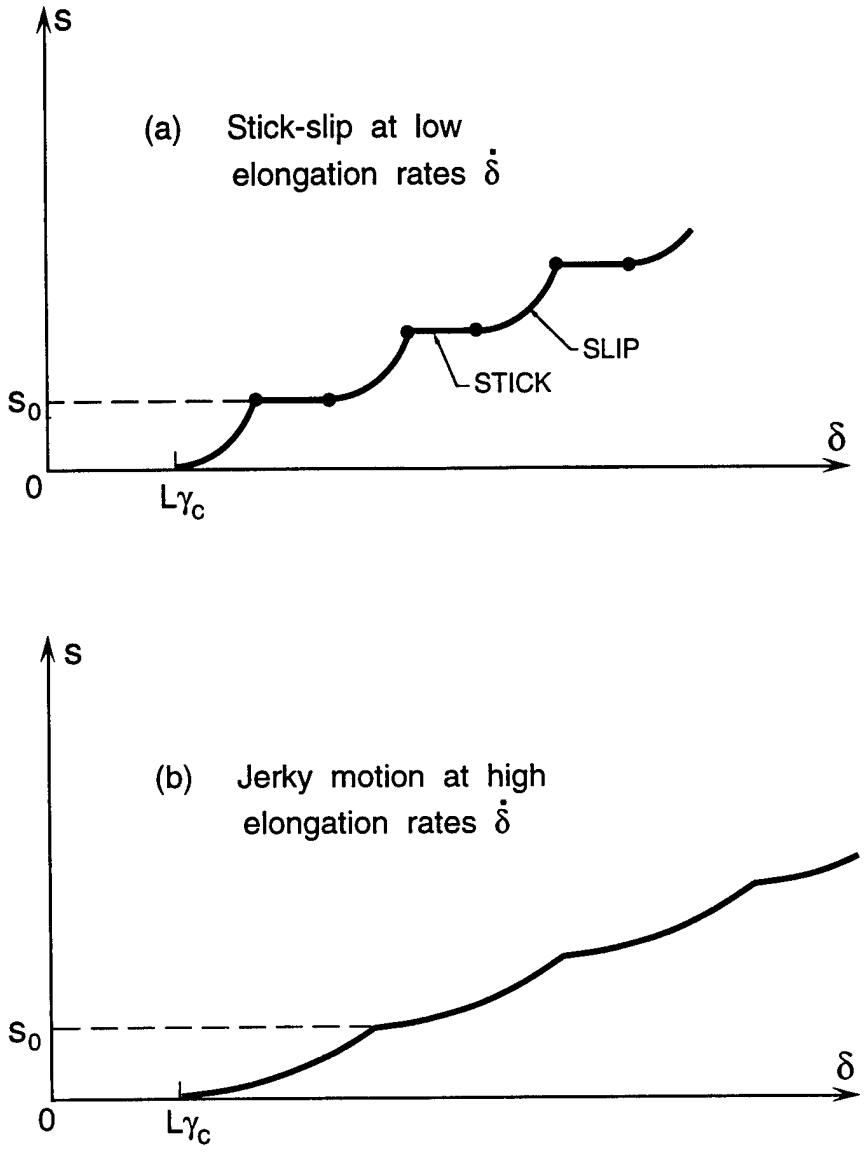

Figure 10. Phase boundary motion $s = s(\delta)$, $\delta = \dot{\delta}t$, at low and high elongation rates $\dot{\delta}$.

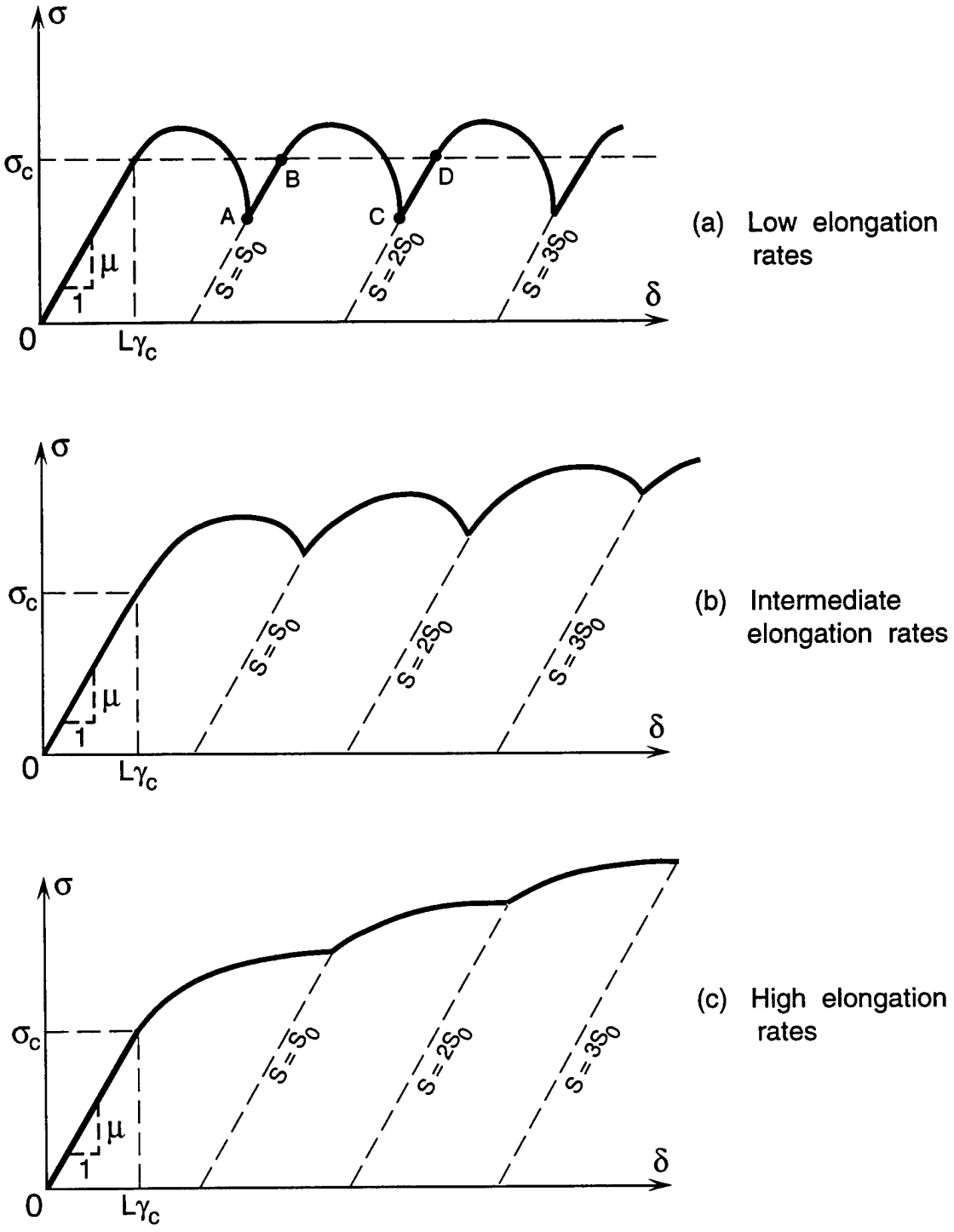

Figure 11. Stress - elongation curves for nonhomogeneous kinetics at various elongation rates.